Energy

Energy Harvesting Footwear

H. Akay, R. Xu, S.-G. Kim
Sponsorship: SUTD

Most portable electronic devices are power-limited by battery capacity, and recharging these batteries often interrupts the user's experience with the device. This product presents an alternative to powering portables by converting regular human walking motion to electricity. The shoe design harvests electric power using rubber lungs, distributed in the sole of a running shoe, to drive a series of micro-turbines connected to small DC motors.

The number and position of lungs are optimized to harvest the maximum airflow from each footstrike. The rubber lungs exhale when compressed and inhale during decompression. The turbine enclosure is designed symmetrically so that regardless of the direction of flow, the turbines continue to spin in the same direction. Therefore, energy is harvested during both stepping and lifting-off of the foot.

A prototype shoe was fitted on the right foot of a 75-kg test subject and produced an average continuous power of 90 mW over a 22.4 Ω load during walking at 3.0 mph. Ongoing research includes applying this design to a fully functional boot that transmits GPS coordinates, powered solely by the user's footsteps.

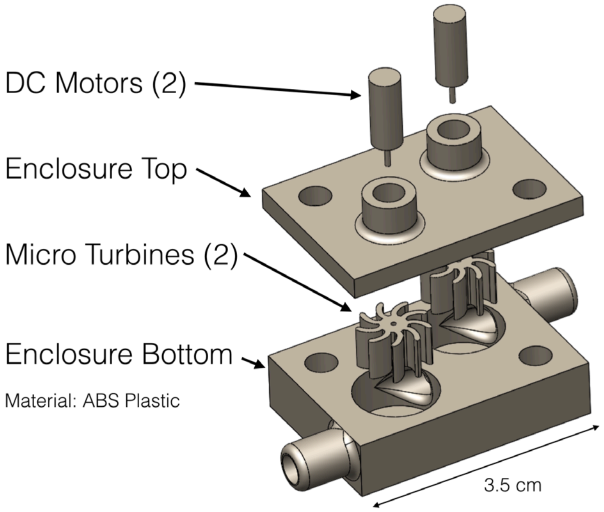

▲ Figure 1: Exploded view of dual-turbine air harvester assembly.

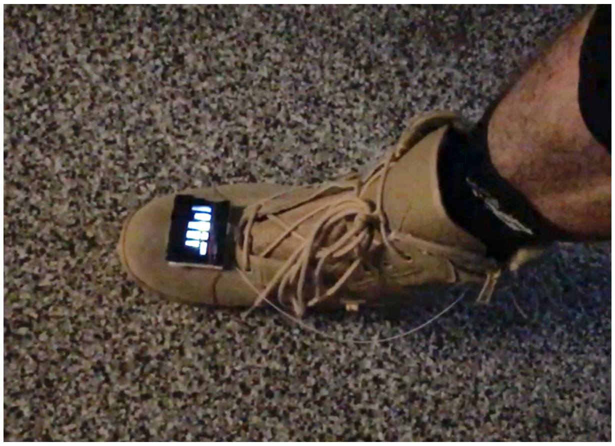

▲ Figure 2: MIT Logo illuminated by a single footstep.

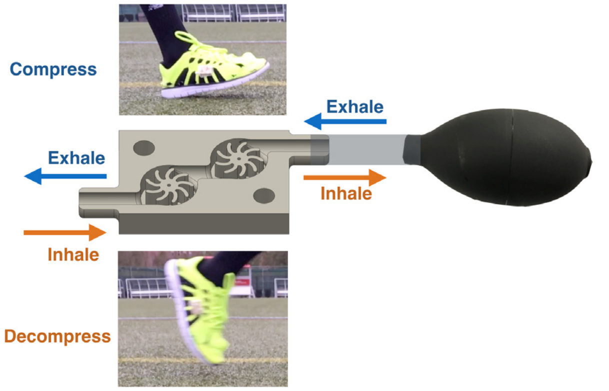

▲ Figure 3: Pump system inhales and exhales, driving turbines continuously

MEMS Energy Harvesting from Low-Frequency and Low-Amplitude Vibrations

R. Xu, H. Akay, S.-G. Kim

Sponsorship: MIT-Singapore University of Technology and Design International Design Center

Vibration energy harvesting at the micro-electrical-mechanical system (MEMS) scale will promisingly advance exciting applications such as wireless sensor networks and the Internet of Things by eliminating troublesome battery-changing or power wiring. On-site energy generation could be an ideal solution to powering a vast number of distributed devices usually employed in these systems. To enable the envisioned battery-less systems, a fully assembled energy harvester at a size of a quarter-dollar coin should generate robustly 101~102μW of continuous power from ambient vibrations (mostly less than 100 Hz and 0.5 g acceleration) with wide bandwidth. We are inching close to this goal in terms of power density and bandwidth, but not in terms of low-frequency and low-amplitude operations. Our previous research with nonlinear resonating bridge-structure-based energy harvesters achieved 2.0 mW/mm3 power density with >20% power bandwidth. However, they were operated with input vibrations of >1 kHz at 4 g, which practically limits the use of this technology for harvesting energy from real environmentally available vibrations. Many believed this is an inherent limitation imposed on the MEMS-scale structures.

We approached this problem with a buckled-beam-based bi-stable nonlinear oscillator. Compared to mono-stable nonlinear oscillations, we found bi-stable oscillations could bring more dynamics phenomena to help reduce the operating frequency. An electromechanical lumped model has been built to simulate the dynamics of the clamped-clamped buckled beam based piezoelectric energy harvesters. A meso-scale prototype verified the theoretical prediction, showing that the same energy harvester in a bi-stable configuration generated more power than the mono-stable configuration at lower frequencies. Residual stress-induced buckling was proposed and implemented through micro-fabrication to build the MEMS energy harvester. The multi-layer bridge structure has employed compressive residual stress in the micro-fabricated thin-films to reach overall compression and balanced stress distribution with respect to the neutral axis. As a main control parameter, the total compression can be tuned to exceed the critical buckling load and induce buckling. The buckled beam oscillates nonlinearly at large amplitude to maintain a wide bandwidth at much lower frequencies. The MEMS prototype of a quarter-dollar coin size (Figure 1) has been built and is being tested. The preliminary testing shows an order-of-magnitude-lower operating frequency range than the same sized mono-stable device we previously developed (Figure 2).

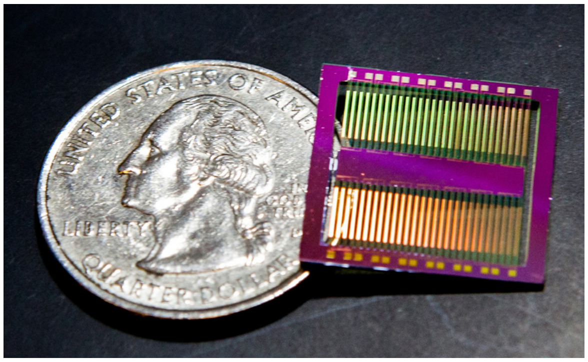

▲ Figure 1: The quarter-dollar coin-sized MEMS energy harvester (18mm × 18mm). The harvester consists of arrays of buckled beams coupled with a central proof mass.

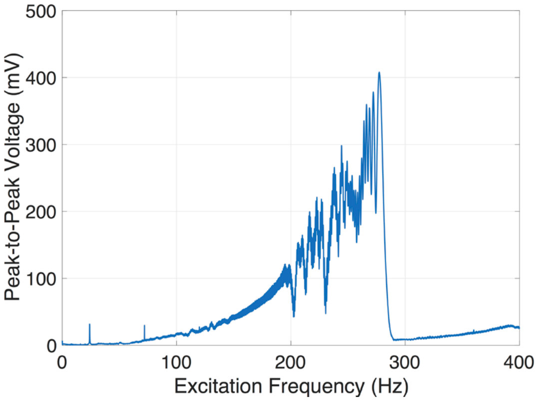

▲ Figure 2: Frequency response (open-circuit voltage) of the MEMS prototype. The input vibrations from the electromagnetic shaker swept from 20Hz to 1000Hz at 0.5g.

FURTHER READING

- R. Xu and S.-G. Kim, "Modeling and Experimental Validation of Bi-Stable Beam Based Piezoelectric Energy Harvester," *Energy Harvesting and Systems*, 2016.
- R. Xu and S.-G. Kim, "Low-Frequency, Low-G MEMS Piezoelectric Energy Harvester," presented at *PowerMEMS 2015*, Boston, MA, 2015.

Broadband Acoustic Energy Harvesting via Synthesized Electrical Loading

N. M. Monroe, J. H. Lang, A. P. Chandrakasan

Sponsorship: Ferrovial, S. A.

With the rise of the Internet of Things and connected devices, the need for self-powered wireless sensor nodes is ever increasing. One promising technology for self-powered sensor nodes in noisy environments is acoustic energy harvesting: deriving energy from ambient sound. Current acoustic energy harvester designs have limited performance; they are typically based on resonant structures, yielding narrowband energy collection and therefore low energy collection from broadband noise sources. In addition, current acoustic energy harvesters tend to the micro-electro-mechanical scale (square microns), with consequently low power outputs. This work addresses the size and bandwidth limitations of such harvesters. A large-scale acoustic energy harvester is designed based on piezoelectric polyvinylidene fluoride (PVDF) film tens of square cm in size, with the potential to scale further.

An energy-based dynamics analysis of such a system driven by an acoustic source yields an equivalent electromechanical resistor-inductor-capacitor (RLC) circuit model and subsequently a Thévenin equivalent model, looking into the piezoelectric element's terminals. Optimal broadband energy harvesting is achieved with a conjugate matched load over broad a frequency range. Such a load is realized as a combination of resistive and negative capacitive impedances. We realize this load initially with operational amplifier circuitry and later losslessly (in theory) using power factor correction-like switched H-bridge circuitry, with control algorithms to force a transfer function impedance of voltage and current. Essentially reactive power is invested in exchange for an increase in real power.

The harvester prototype has been fabricated (see Figure 1) and electromechanical model validated experimentally (see Figure 2). The load circuitry is in initial stages of testing, with a focus on broadband energy harvesting between 50-1000 Hz.

A successful result could pave the path towards acoustically powered sensor nodes, particularly in the case of broadband noisy environments such as airports and highways. There is also potential for application in the context of noise isolation.

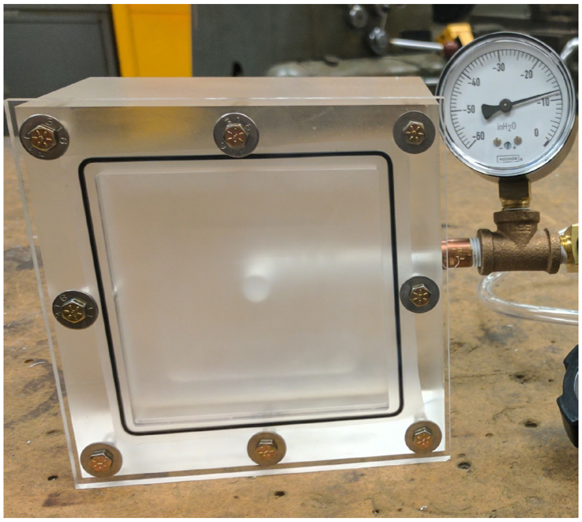

▲ Figure 1: Assembled acoustic energy harvester with active collection area of 100 cm².

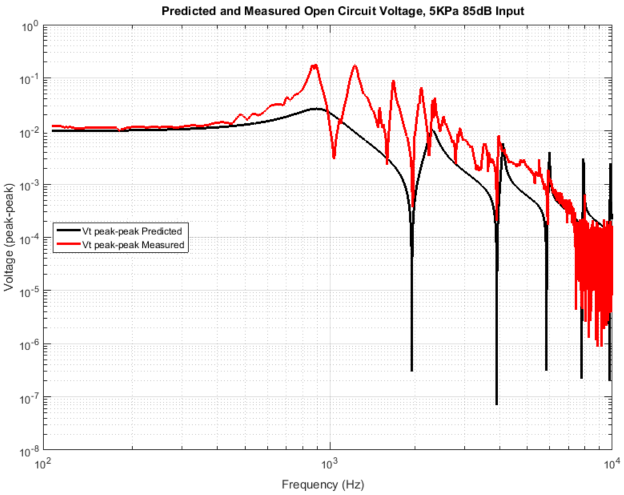

▲ Figure 2: Modeled (black) and measured (red) open circuit voltage of harvester with 85 dB acoustic input. Model considers only first mode of film motion.

FURTHER READING

- M. Pillai, "A Review of Acoustic Energy Harvesting," *International J. Precision Engineering and Manufacturing*, vol. 15, no. 5, 949-965, May 2014.
- S. C. Chang, M. Ocalan, J. Pabon, and J. H. Lang, "Harvesting Energy from Multi-Frequency Vibrations with a Tunable Electrical Load," in *Proceedings PowerMEMS*, 72-75, 2012.
- U. Korde, M. Wickersham, and S. Carr, "The Effect of a Negative Capacitance Circuit on the Out-of-Plane Dissipation and Stiffness of a Piezoelectric Membrane," *Smart Materials and Structures*, vol. 17, 035017, 2008.

MEMS-Based Energy Harvesting System for Machine Health Monitoring

A. Shin, U. Radhakrishna, J. H. Lang, A. P. Chandrakasan

Sponsorship: Analog Devices, Inc.

Vibration-based machine health monitoring provides an effective method of tracking the real-time performance of machines to enable predictive maintenance and avoid machine downtime. Sensors are attached to the vibrating parts that can provide data indicative of machine health. The key challenges to powering such systems are building sensors that can operate at low vibration signals, tolerance to manufacturing variations, a small form-factor, designing low-power electronics for battery-less operation, and efficient power extraction.

To support such systems, a Lorentz-force-based micro-electrical-mechanical (MEMS) energy harvesting system is proposed that can extract 50 uW from machine vibrations around 50 Hz with external acceleration in the range of 0.2-1 g. The harvester consists of a spring-mass system fabricated using a standard Si-MEMS process that oscillates under external vibrations. Magnets embedded in the mass create time-varying magnetic flux during their translational motion. Voltage is induced in windings placed above and below the plane of motion of the spring-mass system in accordance with Faraday's Law. The harvester is designed to have a matched translational resonance frequency of 50 Hz to maximize power extraction, with higher-frequency alternate resonant modes. The geometry parameters are optimized to achieve a power output of 100 uW, while retaining compactness and mechanical stability. The associated power electronics is designed to deliver 50 uW to the load at a 1.8-V regulated output voltage. A boost converter based on an H-bridge topology is implemented to perform impedance tuning and reactive power conditioning for maximizing power extraction under 5% variation in harvester-resonant frequency due to manufacturing tolerances. The circuit also achieves cold-startup using a Meissner-oscillator topology that can start from low voltages of ~100 mV under 5% off-resonance conditions. The integrated circuit implemented in the TSMC 180-nm process can be co-packaged with the harvester and forms a compact energy harvesting system solution for machine health monitoring.

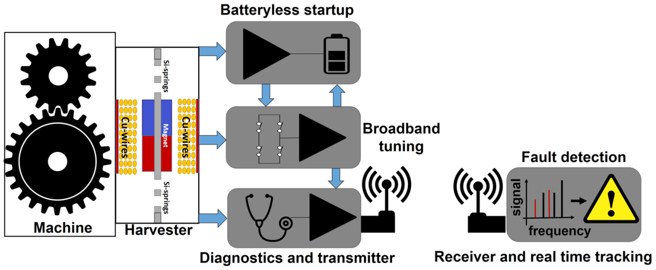

▲ Figure 1: System architecture for a MEMS-based energy harvester and power-conditioning circuit targeted for machine health monitoring. The electronics includes battery-less startup, frequency tuning, and boost conversion to a 1.8-V output voltage.

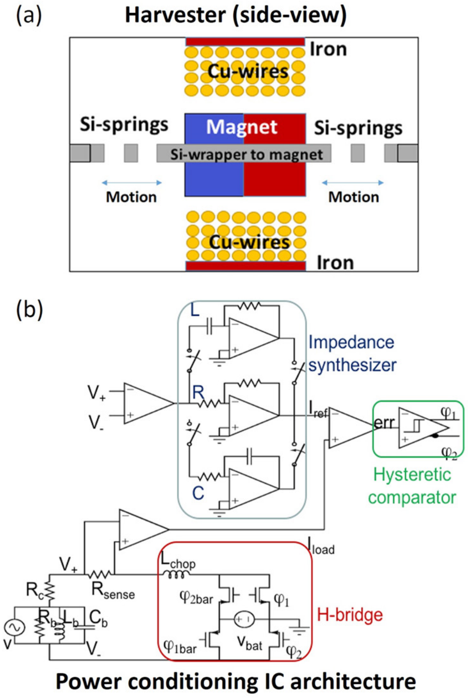

▲ Figure 2: (a) A cross-sectional schematic of the MEMS electromagnetic harvester showing the magnet as a proof mass and the MEMS springs that support magnet motion during external vibrations. (b) The circuit architecture showing the H-bridge topology to achieve impedance matching and efficient charge transfer to the load battery.

FURTHER READING

- Y. Tan, Y. Dong, and X. Wang, "Review of MEMS Electromagnetic Vibration Energy Harvester," *J. Microelectromechanical Systems*, vol. 26, no. 1, 1-16, Feb. 2017.

Use of the Bias Flip Technique in Vibration Energy Harvesting

S. Zhao, D. Buss, J. H. Lang

Harvesting ambient vibration energy through piezoelectric (PZ) energy harvesting devices (EHDs) can provide power for low-power wireless sensor nodes. In order to maximize harvested power at a single frequency, a high-Q resonator is required. However, in most practical applications, the source vibration frequency varies with time, and output power drops dramatically as the source vibration frequency deviates from the resonant frequency.

Our research shows that the resonant frequency can be tuned using an electronic circuit called bias flip (BF). Figure 1 shows the diagram of the PZ energy harvesting system with the BF technique. The BF circuit adiabatically flips the voltage across the output capacitor of the EHD in such a way that it cancels the reactive impedance of the mechanical circuit and achieves phase alignment between the output current and voltage. The BF technique was first used to improve the harvested power at resonant frequency. In this research, we explore ways that the BF technique can be used to cancel the internal reactive impedance of the EHD away from the resonant frequency. The goal of this research is to achieve near-optimum output power from a single frequency even when the frequency deviates from the mechanical resonance frequency of the EHD. If the BF were completely adiabatic, we could achieve optimum output power away from resonance. However, parasitic resistances in the switch and the inductor of the BF circuit lead to loss. We have been able to achieve 90% BF efficiency, and this gives some improvements. As shown in Figure 2, we can improve the 3dB bandwidth by ~3x and improve power by ~10x at frequencies 30% above resonance (150 Hz) or below resonance (80 Hz).

The future work is improving harvested power by reducing the influence of circuit parasitics, such as developing alternative BF topologies, redesigning the PZ EHD, and combining BF technique with other approaches.

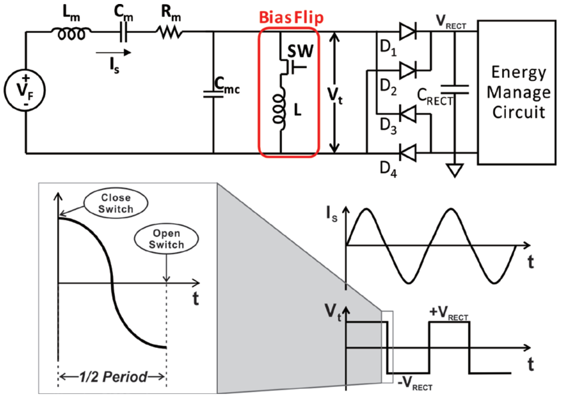

▲ Figure 1: Diagram of the PZ energy harvesting system based on BF technique and associated operation waveforms at resonant frequency.

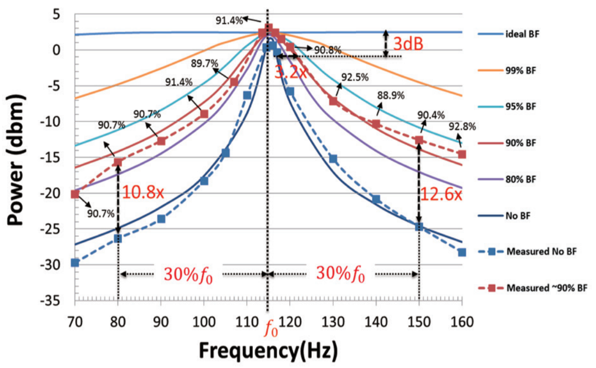

▲ Figure 2: Simulation and experiment results with MIDE V20W PZ EHD for harvested power as a function of vibration frequency with different BF efficiencies under 1-g acceleration.

FURTHER READING

- Y. K. Ramadass and A. P. Chandrakasan, "An Efficient Piezoelectric Energy Harvesting Interface Circuit Using a Bias-flip Rectifier and Shared Inductor," *IEEE J. Solid-State Circuits*, vol. 45, no. 1, 189–204, Jan. 2010.
- S. Zhao, Y. Ramadass, J. H. Lang, J. Ma, and D. Buss, "Bias-Flip Technique for Frequency Tuning of Piezo-electric Energy Harvesting Devices: Experimental Verification," in *Proc. IEEE SOI-3D-Subthreshold Microelectron. Technol. Unified Conf.* (S3S), Oct. 2014.
- S. Zhao, A. Paidimarri, N. Ickes, M. Araghchini, J. Lang, J. Ma, and D. Buss, "Extending the Bandwidth of Piezo-Electric Energy Harvesting through the Use of Bias Flip," in *Proc. IEEE SOI-3D-Subthreshold Microelectron. Technol. Unified Conf. (S3S)*, Oct. 2015.

High-Performance Low-Cost Integrated Micro-Scale Photovoltaics

T. Gu, L. Li, D. Li, B. Jared, G. Keeler, B. Miller, W. Sweatt, S. Paap, M. Saavedra, C. Alford, J. Mudrick, U. Das, S. Hegedus,
A. Tauke-Pedretti, J. Hu
Sponsorship: ARPA-E

High-efficiency, low-cost photovoltaics (PV) techniques beyond Si are critical for new price learning curves and further market penetration of solar technology. By dramatically scaling down the dimensions of multijunction cells to the 100s of microns regime and accordingly concentrating micro-optics, emerging micro-scale PV technologies potentially offer several unprecedented benefits, such as enhanced cell performance, reduced module costs, superior interconnect flexibility, improved heat dissipation, and a thin module form factor.

To fully exploit the PV cell/optic size scaling effects, a novel wafer integrated micro-scale photovoltaic (WPV) approach is developed. Employing low-cost fabrication and integration techniques, such a PV+ technology seamlessly combines the high performance of concentrator PV (CPV) and the low costs of flat panel Si PV. The key notion is a multifunctional Si cell platform that is hybrid-integrated with high-performance multijunction micro-cell arrays and simultaneously provides optical micro-concentration, hybrid photovoltaics, and mechanical micro-assembly functionalities (Figure 1). The Si cell embeds micro-fabricated reflective cavity structures at wafer level to serve as efficient non-imaging micro-optics for concentrating direct sunlight onto III-V cells as well as mechanical alignment features. It also collects diffuse sunlight, a considerable portion of the global radiation that cannot be captured by conventional CPV systems. Our baseline prototypical module (Figure 2) demonstrates a >100% improvement of the concentration-ratio x acceptance-angle product, compared to state-of-the-art CPV technologies, leading to dramatically reduced III-V cell and module fabrication costs, sufficient angular tolerance for low-cost trackers, and an ultra-compact form factor as thin as Si panels, which makes the WPV module compatible with commercial flat panel infrastructures. Analyses and industrial-scale cost modeling indicate that the PV+ approach is able to provide 40-50% and 20-40% more annual energy production per unit area across the USA than conventional Si PV and CPV, respectively, while fully leveraging the module- and system-level cost benefits of low-cost Si PV.

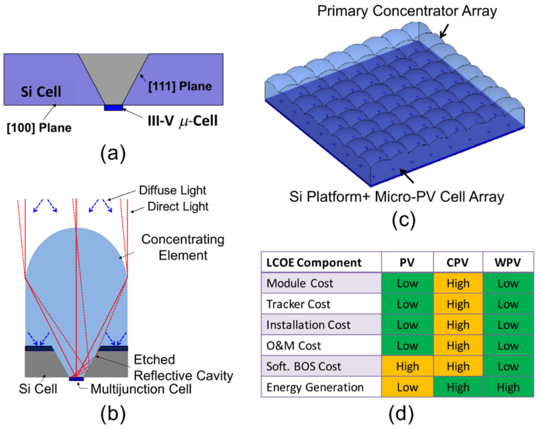

LCOE Component	PV	CPV	WPV
Module Cost	Low	High	Low
Tracker Cost	Low	High	Low
Installation Cost	Low	High	Low
O&M Cost	Low	High	Low
Soft. BOS Cost	High	High	Low
Energy Generation	Low	High	High

▲ Figure 1: A novel wafer-integrated PV+ concept: (a) multi-functional Si cell platform integrated with multi-junction micro-cells, (b & c) a baseline WPV consists of a molded lens array layer, a multi-functional Si cell, and an integrated array of high concentration multijunction micro-cells, (d) comparison of WPV with traditional Si-PV and CPV.

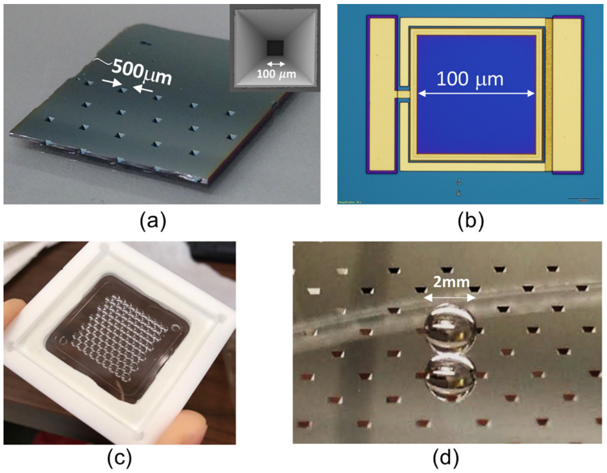

▲ Figure 2: WPV prototypical module: (a) Si platform with etched cavity arrays, (b) III-V micro-cell; (c) packaged molded PDMS primary lens array, (d) self-aligned ball-lens concentrator positioned on a Si cavity.

FURTHER READING

- T. Gu, D. Li, L. Li, B. Jared, G. Keeler, B. Miller, W. Sweatt, S. Paap, M. Saavedra, U. Das, S. Hegedus, R. Birkmire, A. Tauke-Pedretti, and J. Hu, "Wafer-level Integrated Micro-Concentrating Photovoltaics," invited talk at *OSA Light, Energy and the Environment Congress,* Leipzig, Germany, Nov. 2016.

Stored Energy as a Measurable Unit of Radiation Damage in Materials

C. A. Hirst, R. C. Connick, L. Abel, K. Carter, S. Lowder, P. Cao, M. P. Short

Sponsorship: MIT-Singapore University of Technology and Design Collaboration Office, International Design Centre

When particle radiation passes through a material, it can knock host atoms off their lattice sites. This leads to the formation of defects that change the material's properties. The unit currently used to describe radiation damage is the average number of displacements per atom (dpa) in the material. However, this value overestimates the defect population as it does not account for recombination and annihilation of defects following their formation.

The atoms in these defects have an associated energy that is greater than that of atoms in a perfect crystal. We propose to measure the stored energy of the defects through fast differential scanning calorimetry (DSC) and correlated molecular dynamics simulations. This stored "Wigner" energy is determined by the size, number, and type of defects present in the material, thereby accounting for any recombination that has occurred. Knowledge of the true distribution of defects will allow accurate predictions of a material's properties to be made over practical lengths and timescales.

Samples were prepared using electron beam physical vapor deposition (ebeam PVD) of pure Al onto the SiN-based chip. A shadow mask was utilized to restrict the deposition to a 50-µm-spot size within the analysis region of a Mettler Toledo UFS1 twin calorimeter chip (see Figure 1). The chip and sample were then irradiated with 3.4MeV He^{2+} ions to a fluence of 3.5 x 10^{18} ions/cm2 in the CLASS tandem ion accelerator.

These were then analyzed by heating from room temperature to 450˚C at 10,000Ks^{-1} in a Mettler Toledo Flash DSC. The difference between the first (irradiated) and subsequent (baseline) heating curves is the difference between defected and "perfect" material. This represents the stored energy released by the sample during heating, i.e., the annealing out of the irradiation induced defects (see Figure 2). These initial results are proof of the concept with further work including a systematic investigation of irradiation dose versus stored energy and an evaluation of heating rate, irradiation dose rate, and sample preparation effects.

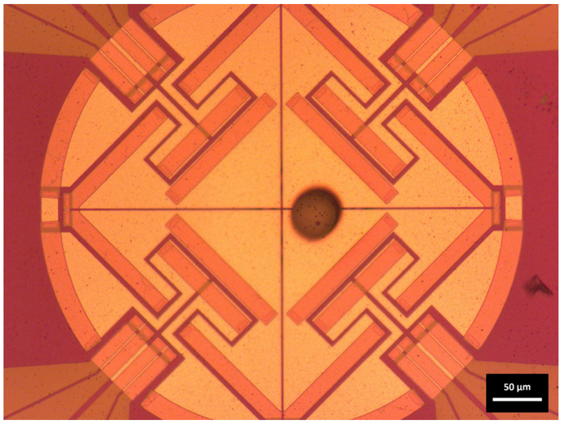

▲ Figure 1: Bright field optical image showing the successful deposition (ebeam PVD) of a 1-µm-thick, ⌀ 50 µm, pure Al sample within the analysis region of a Mettler Toledo UFS1 twin calorimeter chip.

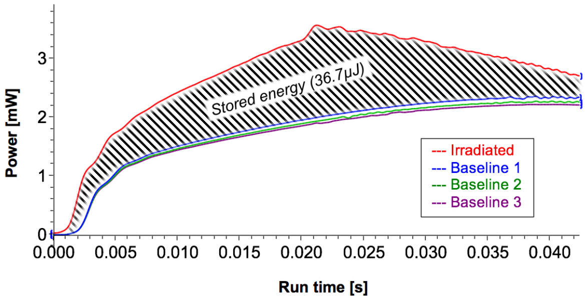

▲ Figure 2: Consecutive heating curves showing the release of energy from the sample during the first (irradiated) heating ramp compared to subsequent (baseline) ramps. Run time is directly proportional to temperature from 30°C to 450°C, with the heating rate 10,000Ks^{-1}.

FURTHER READING

- NSF CAREER Proposal #1654548 "Quantifying Radiation Damage in Metals with Wigner Energy Spectral Fingerprints."
- S. van Herwaarden, E. Iervolino, F. van Herwaarden, T. Wijffels, A. Leenaers, V. Mathot, "Design, Performance and Analysis of Thermal Lag of the UFS1 Twin-Calorimeter Chip for Fast Scanning Calorimetry using The Mettler-Toledo Flash DSC 1," *Thermochimica Acta* vol. 522, 46-52, 2011.
- C. Schick and V. Mathot, Eds., "Fast Scanning Calorimetry," *New York, Springer*, 2016.

Interdigitated Electrodes for *in situ* Measurements of Electrochemical Devices

J. G. Swallow, T. Defferriere, H. L. Tuller, K. J. Van Vliet
Sponsorship: U.S. Department of Energy Office of Science

Solid oxide fuel cells (SOFCs) and lithium ion batteries are electrochemical energy conversion and storage devices that rely heavily on materials known as non-stoichiometric oxides. This class of oxides can tolerate very large point defect concentrations that enable useful properties including ionic conductivity or gas exchange reactivity. For SOFCs, ionic conductivity is enabled by transport of oxide ions through a vacancy-mediated mechanism, while oxygen gas exchange operates through incorporation of oxide ions into existing oxygen vacancy sites. Thus, the electrochemical transport and reactivity properties of non-stoichiometric oxides are highly dependent on oxygen vacancy concentration and kinetics, which depend on environmental conditions including temperature, *T*, and oxygen partial pressure, pO2.

In order to understand the electrochemical performance of oxide materials in the range of environments that might be present in operating devices (e.g., T > 600°C, pO2 between 0.2 and 10-15 atm), it is necessary to measure these properties *in situ*. Thin-films are excellent model systems for this purpose, due to their well-controlled compositions and simple geometries that are optimal for rapid testing with electrochemical impedance spectroscopy (EIS). To measure the electronic and ionic conductivity of such films, electrodes that maximize signal to noise are required. Specifically, interdigitated electrodes (IDEs) like those shown in Figure 1 can significantly improve the signal-to-noise ratio over that of simple electrodes and may be fabricated with extreme reproducibility and precision using photolithography.

To fabricate devices like the one shown in Figure 1, photolithography was used to pattern 40-µm IDE photoresist masks onto the surface of an oxide film grown by pulsed laser deposition on a single crystal substrate. Platinum electrodes were then sputtered onto these masks. This was followed by chemical lift-off to remove the remaining photoresist. Such devices may be tested using EIS under a range of conditions, including varied temperatures or gas atmospheres. Spectra like the one shown in Figure 2 can be used to understand how the ionic and electronic transport characteristics of the oxide film are affected by environmental conditions of temperature and oxygen partial pressure.

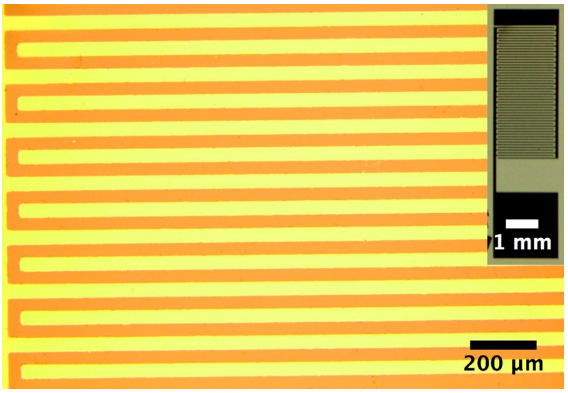

▲ Figure 1: IDEs fabricated by photolithography on oxide films grown by pulsed laser deposition. The inset shows a low magnification view of device geometry.

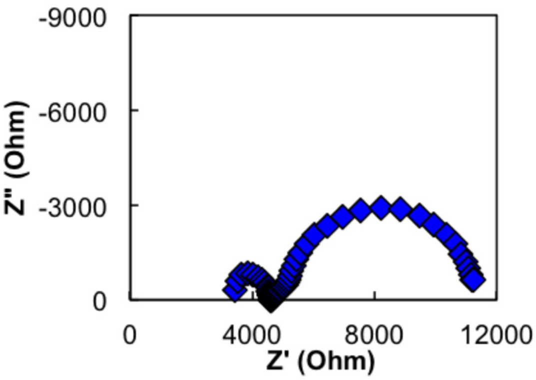

▲ Figure 2: EIS of a non-stoichiometric oxide film taken using IDEs like those shown in Figure 1 at 640°C. IDEs provide large effective electrode area that enhances signal-to-noise.

FURTHER READING

- H. L. Tuller and S. R. Bishop, "Point Defects in Oxides: Tailoring Materials through Defect Engineering," *Annual Reviews of Materials Research*, vol. 41, no. 1, 369-398, 2011.
- J. L. Hertz and H. L. Tuller, "Electrochemical Characterization of Thin Films for a Micro-Solid Oxide Fuel Cell," *J. Electroceramics*, vol. 13, 663-668, 2004.

Controlling the Phase and Properties of Functional Oxides by Electrochemical Potential

Q. Lu, S. R. Bishop, G. Vardar, H. L. Tuller, B. Yildiz
Sponsorship: NSF

Functional oxides play an important role in the performance of novel electronic devices and energy-storage technologies owing to their highly tunable properties, which can be largely altered via external stimuli. The change of physical properties, including electrical conductivity and magnetism, induced in a controlled and non-volatile fashion can potentially enable emerging information-storage devices. We have developed a new means of tuning the crystal structure and electronic structure by using electrochemical potential to control the oxygen content in the oxide. The aim is to trigger phase transition electrochemically and obtain distinctly different physical and chemical properties. We employed advanced *in situ* material characterization tools to reveal the mechanism of electrochemically induced oxide phase transitions. Our findings can potentially guide the design of new types of electronic devices based on this mechanism.

We implemented this novel method of controlling oxide properties in model system of $SrCoO_x$, which can take two different crystal structures depending on the oxygen stoichiometry, i.e., oxygen-deficient layered brownmillerite-structured $SrCoO_{2.5}$, which is a semiconductor, and oxygen-rich perovskite-structured $SrCoO_3$, which is metallic. By using *in situ* X-ray diffraction, we could probe the electrochemically triggered phase transition between these two crystal structures. We found that an electrochemical bias of merely 25 mV was sufficient to trigger the phase transition, while it is very difficult to obtain this phase transition by conventional chemical methods. We further utilized *in operando* synchrotron-based X-ray spectroscopic tools to depict the evolution of the electronic structure of $SrCoO_x$ during the phase transition. The transition allows for a large change in the electronic structure and electronic conductivity.

This electrochemical method of controlling phase and properties is applicable to a wide range of oxides that have multivalancy and associated distinct phases. We have recently applied this strategy to another functional oxide of importance to electronic devices, i.e., vanadium oxide, VO_x. We revealed a new, electrochemically controlled branch of metal-to-insulator transition between two VO_x phases. The transition can be triggered at a wide range of temperatures, from room temperature to several hundreds of Celsius degrees. This approach opens a new route for designing new "ionotronic" (i.e., "ionic + electronic") devices based on VO_x.

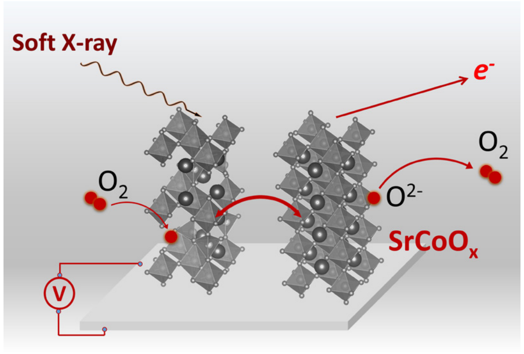

▲ Figure 1: Schematic showing the electrochemically controlled phase change and property control (exemplified by $SrCoO_x$). Oxygen ions are incorporated or removed from the oxide structure depending on the polarity of the biases applied. Soft X-ray spectroscopy is used to probe the phase and electronic structure change during this process.

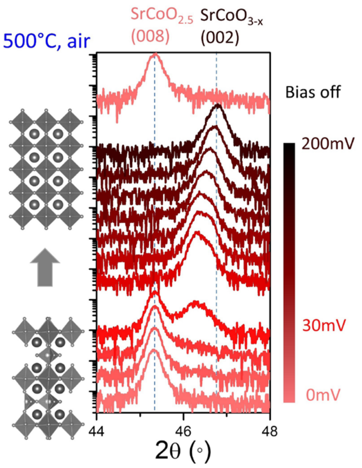

◀ Figure 2: *In situ* X-ray diffraction pattern on $SrCoO_x$. Electrochemical bias was applied to alter the phase and crystal structure from $SrCoO_{2.5}$ to $SrCoO_{3-x}$, which leads to the change in the shown peak position.

FURTHER READING

- Q. Lu and B. Yildiz, "Voltage-Controlled Topotactic Phase Transition in Thin-Film SrCoOx Monitored by *In Situ* X-ray Diffraction," *Nano Lett.*, vol. 16, 1186-1193, 2016.
- Q. Lu, Y. Chen, H. Bluhm, and B. Yildiz, "Electronic Structure Evolution of SrCoOx during Electrochemically Driven Phase Transition Probed by *in Situ* X-Ray Spectroscopy," *J. Physical Chemistry C*, vol. 120, 24148-24157, 2016.

Electro-Chemo-Mechanical Studies of Perovskite-Structured Mixed Ionic-Electronic Conducting $SrSn_{1-x}Fe_xO_{3-x/2+\delta}$

C. S. Kim, S. R. Bishop, N. H. Perry, H. L. Tuller

Sponsorship: Skolkovo Foundation

High efficiency and fuel flexibility make solid oxide fuel cells (SOFCs) attractive for conversion of fuels to electricity. Reduced operating temperatures, desirable for reduced costs and extended operation, however, result in significant losses in efficiency. This loss has been traced primarily to slow cathode surface reaction kinetics. In this work, we extend previous studies on the promising mixed ionic and electronic conducting perovskite-structured $SrTi_{1-x}Fe_xO_{3-x/2+\delta}$ (STF) materials system, whose exchange kinetics were correlated with the minority electron charge density by replacing Ti with Sn, due to its distinct band structure and higher electron mobility.

Oxygen nonstoichiometry and the defect chemistry of the $SrSn_{1-x}Fe_xO_{3-x/2+\delta}$ (SSF) system were examined by thermogravimetry as a function of oxygen partial pressure in the temperature range of 973-1273 K. Marginally higher reducibility was observed compared to corresponding compositions in the STF system. The bulk electrical conductivity was measured in parallel to examine how changes in defect chemistry and electronic band structure, associated with the substitution of Ti by Sn, impact carrier density and ultimately electrode performance. Bulk chemical expansion was measured by dilatometry as a function of oxygen partial pressure, while surface kinetics were examined by means of AC impedance spectroscopy. The electro-chemo-mechanical properties of SSF were found not to differ significantly from the corresponding composition in STF. Key thermodynamic and kinetic parameters for $SrSn_{0.65}Fe_{0.35}O_{2.825+\delta}$ (SSF35) were derived, including the reduction enthalpy, electronic band gap, anion Frenkel enthalpy, oxygen vacancy migration energy, and electron and hole mobilities. Though slightly shifted by the larger size of Sn, the defect equilibria and the cathode area specific resistance differed only in a limited way from that in STF. This small difference was attributed to properties being largely dominated by Fe and not by the substitution of Ti with Sn.

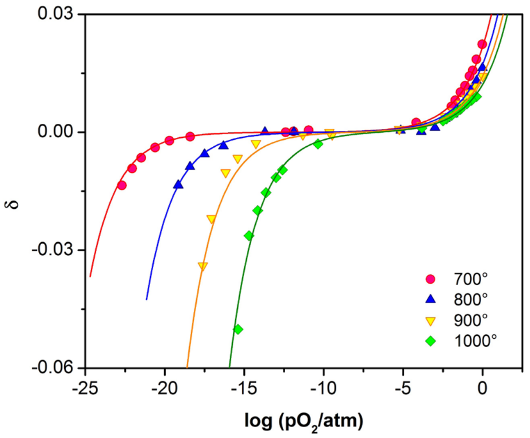

▲ Figure 1: Oxygen nonstoichiometry δ as a function of pO_2 and temperature for SSF35.

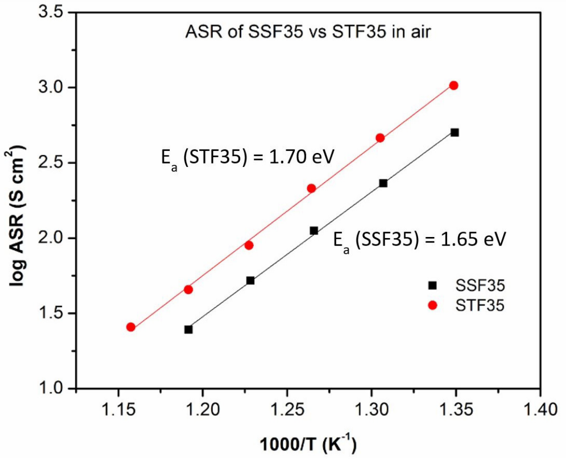

▲ Figure 2: Comparison of temperature dependence of area specific resistance of SSF35 and STF35 thin-film electrodes.

FURTHER READING

- W. Jung and H. L. Tuller, "A New Model Describing Solid Oxide Fuel Cell Cathode Kinetics: Model Thin Film SrTi1-xFexO3-δ Mixed Conducting Oxides–a Case Study," *Advanced Energy Materials*, vol. 1, 1184–1191, 2011.

Controlling Concentration and Nature of Oxygen Defects in Layered Cuprate-Based Materials by Electrical Bias

C. S. Kim, H. L. Tuller
Sponsorship: Skolkovo Foundation

Both the nature and concentration of oxygen defects in oxide materials can have a significant impact on their physical and chemical properties as well as key interfacial reaction kinetics such as oxygen exchange with the atmosphere, important of sensor, fuel cell and electrolysis cell operation. Most commonly, the desired oxygen defect concentration, or equivalently oxygen nonstoichiometry, is attained in a given material by controlling the oxygen partial pressure and temperature in which it is equilibrated or annealed. This approach, however, is limited by the range of oxygen partial pressures readily experimentally achievable and requires knowledge of the applicable defect chemical model. In this study, we fine-tune oxygen defect concentrations in promising rare earth cuprate (RE_2CuO_4: RE = rare earth) solid oxide fuel cell cathode materials by application of electrical potentials across an yttria-stabilized zirconium supporting electrolyte. These layered perovskites can incorporate both oxygen interstitials and vacancies, thereby broadening the range of investigations. Oxygen nonstoichiometry values are determined by in-situ measurement of chemical capacitance and are compared with corresponding information available for bulk specimens. These studies are expected to provide further insight into the defect and transport mechanisms that support enhanced SOFC cathode performance.

FURTHER READING

- D. Chen and H. L. Tuller, “Voltage-Controlled Nonstoichiometry in Oxide Thin Films: $Pr_{0.1}Ce_{0.9}O_{2-\delta}$ Case Study,” *Advanced Functional Materials*, vol. 24, no. 48, 7638-7644, Dec. 2014.

Utilization of $BaSnO_3$ and Related Materials Systems for Transparent Conducting Electrodes

M. Campion, S. R. Bishop, H. L. Tuller

Sponsorship: NSF

Efficient transparent electrode materials are vital for applications in smart window, LED display, and solar cell technologies. These materials must possess a wide band gap for minimal optical absorption in the visible spectrum while maintaining a high electrical conductivity. Tin-doped indium oxide (ITO) has been the industry standard for transparent electrodes, but the use of the rare element indium has led to a search for better material alternatives. $BaSnO_3$ represents a promising alternative due to its high electron mobility and resistance to property degradation under oxidizing conditions, but the mechanisms by which processing conditions and defect chemistry affect the final material properties are not well understood.

This work seeks to better understand the relationships between processing, defect chemistry, and material properties of $BaSnO_3$, in order to better establish the consistent and controllable use of $BaSnO_3$ as a transparent electrode. To accomplish these goals, methods such as in-situ resistance and impedance monitoring during annealing will be applied. In addition, a variety of novel methods such as the *in situ* monitoring of optical transmission (shown in Figure 1) during annealing and the in-situ monitoring of resistance during physical vapor deposition will be utilized to investigate $BaSnO_3$. Direct measurements of the key constants for the thermodynamics and kinetics of oxidation in donor-doped $BaSnO_3$ will be experimentally determined for the first time. This increase in understanding will provide a predictive model for determining optical properties, carrier concentrations, and electron mobilities in $BaSnO_3$, which may be become increasingly important due to its high electron mobility, high temperature stability, and favorable crystal structure.

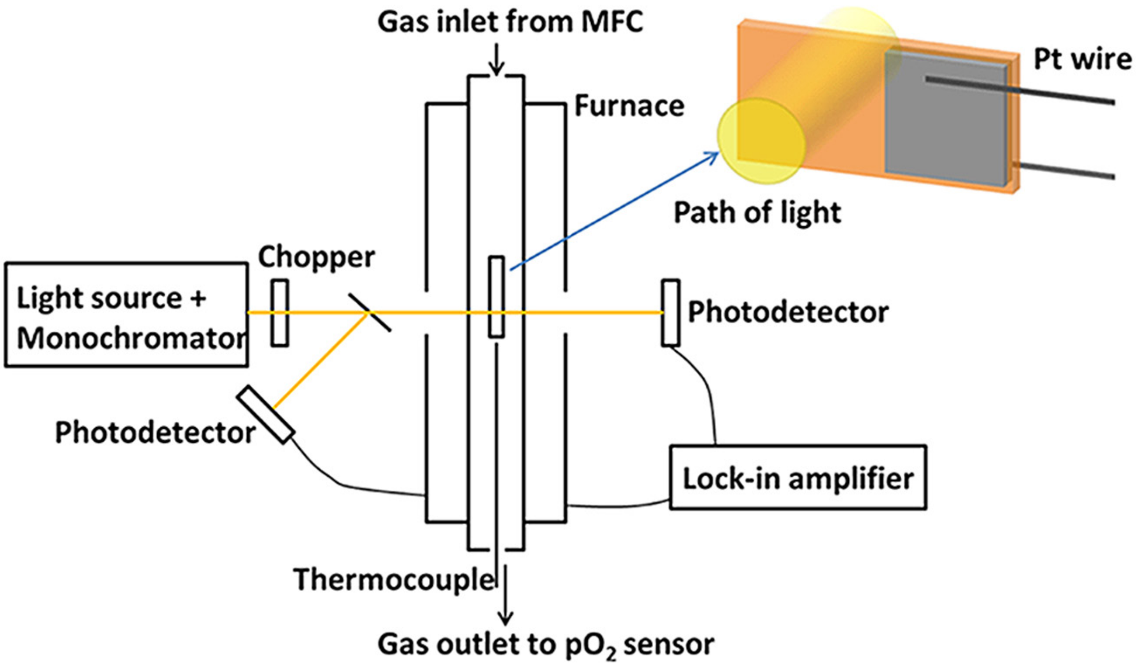

▲ Figure 1: Schematic of experimental setup to be used for simultaneous in-situ measurement of the optical transmission and electrical conductivity of thin-film BaSnO3 samples during annealing under controlled atmosphere and temperature.

FURTHER READING

- D. O. Scanlon, “Defect Engineering of BaSnO3 for High-Performance Transparent Conducting Oxide Applications,” *Phys. Rev. B*, vol. 87, no. 16, 161201, Apr. 2013.
- J. J. Kim, S. R. Bishop, N. J. Thompson, D. Chen, and H. L. Tuller, “Investigation of Nonstoichiometry in Oxide Thin Films by Simultaneous *in situ* Optical Absorption and Chemical Capacitance Measurements: Pr-Doped Ceria, a Case Study,” *Chemistry of Materials*, vol. 26, no.3, 1374-1379, 2014.

Understanding Mechanisms and Optimizing Capacity for Lithium-O_2 Batteries

T. Batcho, D. Kwabi, Y. Shao-Horn, C. V. Thompson

Sponsorship: Skoltech Center for Electrochemical Energy Storage

Lithium-O_2 batteries hold promise for the next generation of electric vehicles and other applications. By reacting oxygen directly with lithium ions to form Li_2O_2 on discharge, they can achieve energy densities 3-5 times higher than current lithium-ion batteries. Because Li_2O_2 forms an electrically insulating film during discharge that passivates the electrode surface, obtaining optimal volumetric capacities requires an understanding of the mechanisms that control Li_2O_2 film formation.

High volumetric capacities can be achieved by promoting the growth of large toroidal deposits of Li_2O_2 as opposed to thin-films, which cut off cell discharge prior to full void space filling of the electrode. Li_2O_2 can form by a surface pathway involving two-electron transfers into a film or by a solution pathway involving a one-electron transfer to create solvated LiO_2 that chemically forms toroidal Li_2O_2. We study the mechanisms of nucleation and growth by the surface pathway to promote more efficient void filling. Potentiostatic discharges provide useful information about the kinetics of the film formation as the driving force for Li_2O_2 is fixed, which allows the application of existing models for electrodeposition to our system to extract rates of surface nucleation and growth. Our initial efforts have focused on performing potentiostatic discharges on carbon paper in a standard cell. This method shows that potential determines the rate of film growth (Figure 1), but it provides no means to separately characterize the mechanisms of the surface and solvent processes.

To distinguish current that forms Li_2O_2 in solution from current that forms Li_2O_2 on the electrode, we use the rotating ring disk electrode technique (RRDE). RRDE reduces oxygen at an inner disk electrode to form insoluble Li_2O_2 on that electrode or soluble LiO_2 that is swept to an outer ring electrode by a convection current created by rotating the setup (Figure 2). Since we directly measure the amount of soluble species at the ring, we can calculate the amount of Li_2O_2 formed by the surface pathway. This allows us to model the nucleation and growth kinetics of the surface film formation. We use RDDE to study how solvent properties and potential govern surface film growth kinetics, which will be key in achieving high void-filling high volumetric capacity Li-O_2 batteries.

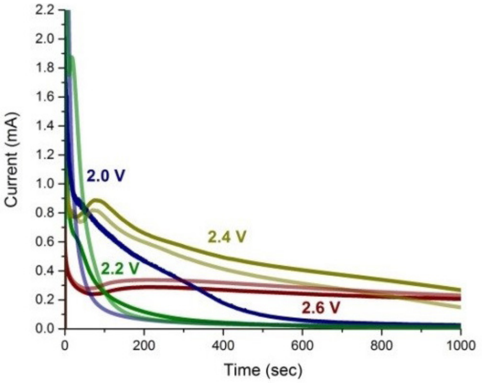

▲ Figure 1: Current transients for potentiostatic discharges at a range of potentials in 0.1 M $LiClO_4$ DMSO on carbon paper. Peaks occur at longer times at higher potentials (lower overpotentials), suggesting slower nucleation/growth rates.

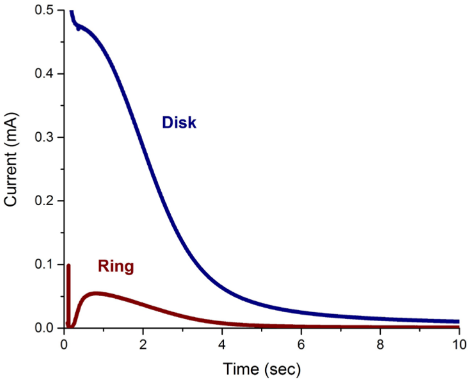

▲ Figure 2: Disk current transient (blue) and corresponding ring current transient (red) for a 2.4V discharge in 0.1 M $LiClO_4$ DMSO. The ring current gives a measure of the amount of soluble species produced on the disk.

FURTHER READING

- R. R. Mitchel, B. M. Gallant, Y. Shao-Horn, and C. V. Thompson, "Mechanisms of Morphological Evolution of Li_2O_2 Particles during Electrochemical Growth," *J. Physical Chemistry Lett.*, vol. 4, no. 7, 1060, Mar. 2013.
- D. G. Kwabi, M. Tulodziecki, N. Pour, D. M. Iitkis, C. V. Thompson, and Y. Shao-Horn, "Controlling Solution-Mediated Reaction Mechanisms of Oxygen Reduction using Potential and Solvent for Aprotic Lithium-Oxygen Batteries," *J. Physical Chemistry Lett.*, vol. 7, no. 7, 1204–1212, Mar. 2016.

Kinetic Studies of the Initial Lithiation Si Thin-Film Anodes

J. Miao, C. V. Thompson

Sponsorship: SMART, Skoltech Center for Electrochemical Energy Storage

Li-ion batteries are the most widely used secondary batteries. Researchers have been aiming for larger capacity and energy density, better cycling performance, and safer operation. Also, in response to the trend toward miniaturized device development in the electronic and health industries, all-solid-state planar microbatteries have received special attention because they can be integrated with complementary metal-oxide semiconductor (CMOS) technology and offer improved safety since no liquid electrolyte is used. Among known anode materials, Si is a promising candidate for applications in microbatteries. It has extraordinarily high volumetric and gravimetric capacities (8375 Ah/cm^3, 3579 Ah/kg), along with a low discharge potential and thus a high energy density. The reason that Si exhibits such high capacities is related to its alloying mechanism during lithiation and delithiation. Quite different from conventional intercalation anodes, the lithiation of amorphous Si proceeds by bond breakage and formation of new atomic scale structures in a series of phase transformations. Unfortunately, this mechanism also leads to a large volume expansion and can lead to battery failure. To explore the alloying lithiation process of Si thin-films and better understand the reaction mechanisms and the potential for material optimization, electrochemical methods and material analysis were used to study the irreversible phase transition that occurs in the first lithiation cycle and the change in transformation mechanisms between cycles.

It was found that the current vs. time plot for the first lithiation in the first charge-discharge cycle (Figure 1, black curve) during potentiostatic lithiation shows a step feature that cannot be explained using the single phase diffusion model that is often envisioned for the lithiation process. The time at which the step occurs increases with increasing film thickness, suggesting a transformation mechanism involving the motion of a planar interface, as shown in Figure 2(a). The behavior leading to the step can be divided into two regimes, with the curve before the step showing a square root of time dependence and the curve after the step fitting an exponential decay. This division is consistent with diffusion limited thickening of the lithiated phase (Figure 2a), followed by elimination of the Li concentration gradient in the fully transformed film. In the second lithiation cycle, the step feature is absent (Figure 1, red curve). This absence suggests that after the transformation in cycle 1, the single phase diffusion model applies (Figure 2b). Therefore, it is concluded that the two-phase coexistence and interface propagation process that occurs in cycle 1 leads to an at least partly irreversible expansion of the Si structure during cycle 1. Modification of this process might allow optimization of battery performance in subsequent cycles.

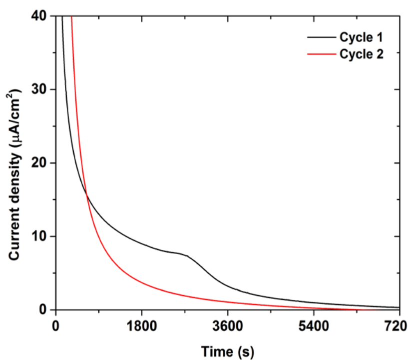

▲ Figure 1: Current density vs. time plots for a 315- nm-thick amorphous Si (a-Si) thin-film in cycle 1 and cycle 2 in potentiostatic tests.

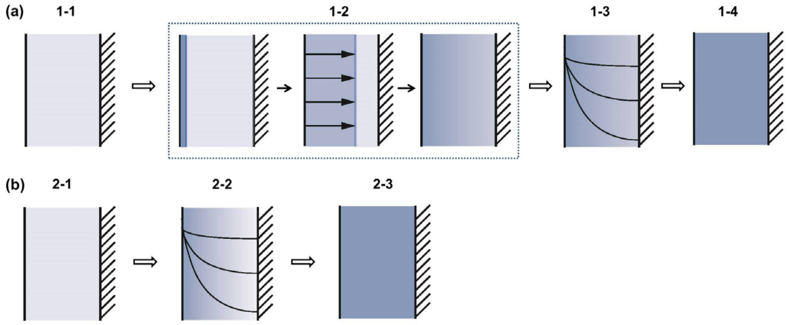

▲ Figure 2: (a) Cycle 1 and (b) Cycle 2 lithiation models under a constant potential for a 315-nm- thick a-Si thin-film.

Integrated All-Solid-State Supercapacitors for Si Microsystems

W. Zheng, Q. Cheng, D. Wang, C. V. Thompson
Sponsorship: SMART

Autonomous microsystems require devices for energy storage. Thin-film microbatteries store energy at high density but typically operate at low power, while capacitors can operate at high power but do not provide high density storage. Autonomous microsystems, such as autonomous sensors, require both high energy density storage for efficient use of space and high power for broadcast of data. We are developing all-solid-state thin-film microbatteries, discussed elsewhere, and nanowire-array supercapacitors that can be fabricated using the tool set for complementary metal-oxide semiconductor (CMOS) processing.

Solid-state on-chip supercapacitors based on ruthenium oxide coated silicon nanowires were fabricated. Ordered arrays of silicon nanowires were made using metal-assisted anodic etching (MAAE), as in Figure 1. Atomic layer deposition (ALD) was used to form a uniform coating of ruthenium oxide on high-aspect-ratio silicon nanowires at a moderate temperature of 290°C. Coated nanowire electrodes were studied using cyclic voltammetry and charge-discharge tests in a neutral Na_2SO_4 electrolyte, and a specific capacitance of 19 $mFcm^{-2}$ was achieved at 5 mVs^{-1}. Solid-state nanowire capacitors were then fabricated with symmetric face-to-face nanowire arrays separated by a polymer-based solid electrolyte. This device exhibited a specific capacitance as high as 6.5 $mFcm^{-2}$ at 2 mVs^{-1}, as Figure 2 shows. The full device was tested over 10,000 cycles under galvanostatic charge/discharge at 0.4 $mAcm^{-2}$ and showed a retention of 92% of the specific capacitance. The specific capacitance was found to scale with the total nanowire surface area, by controlling the aspect ratios of the wires. The solid-state nanowire-based device also achieved high specific energies without sacrificing power performance.

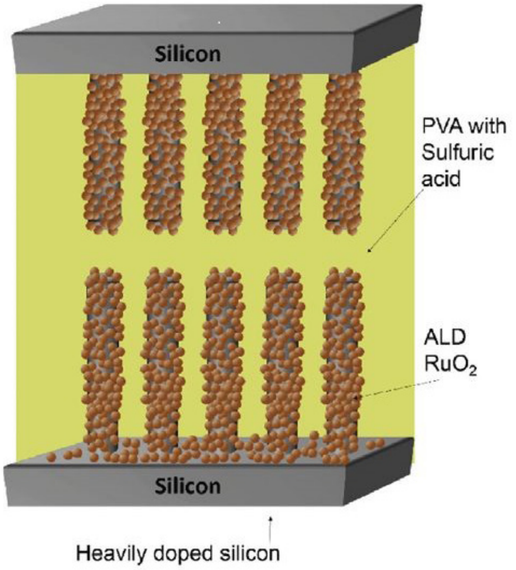

▲ Figure 1: Schematic of the symmetric solid-state on-chip supercapacitor based on RuO_x- coated arrays of silicon nanowires (SWNs).

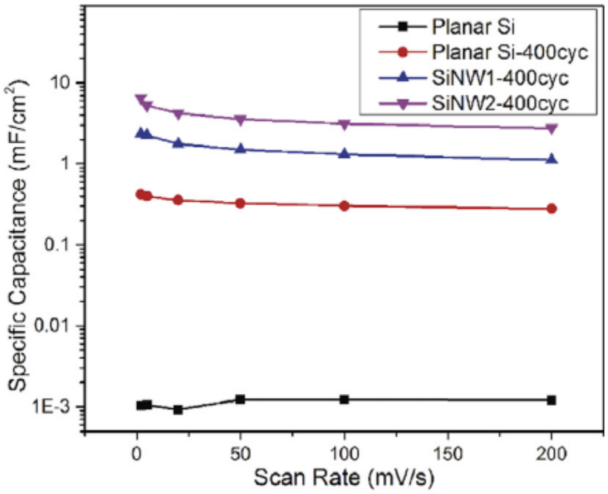

▲ Figure 2: Specific capacity versus scan rate for all-solid-state planar capacitors with and without RuO_x coatings and silicon nanowire capacitors with two different NW aspect ratios.

FURTHER READING

- W. Zheng, Q. Cheng, D. Wang, and C. V. Thompson, "High-Performance Solid-State on-chip Supercapacitors Based on Si Nanowires Coated with Ruthenium Oxide via Atomic Layer Deposition," *J. of Power Sources*, vol. 341, 10, 2017.